Available online at www.sciencedirect.com
ScienceDirect
Journal of Molecular Graphics and Modelling 26 (2007) 643–651
Journal of Molecular Graphics and Modelling
www.elsevier.com/locate/JMGM

Stepwise dissection and visualization of the catalytic mechanism of haloalkane dehalogenase LinB using molecular dynamics simulations and computer graphics

Ana Negri [a], Esther Marco [a], Jiri Damborsky [b], Federico Gago [a,*]

[a] *Department of Pharmacology, University of Alcalá, E-28871 Alcalá de Henares, Madrid, Spain*
[b] *Loschmidt Laboratories, Faculty of Science, Masaryk University, Kotlarska 2, 611 37 Brno, Czech Republic*

Accepted 20 March 2007
Available online 24 March 2007

Abstract

The different steps of the dehalogenation reaction carried out by LinB on three different substrates have been characterized using a combination of quantum mechanical calculations and molecular dynamics simulations. This has allowed us to obtain information in atomic detail about each step of the reaction mechanism, that is, substrate entrance and achievement of the near-attack conformation, transition state stabilization within the active site, halide stabilization, water molecule activation and subsequent hydrolytic attack on the ester intermediate with formation of alcohol, and finally product release. Importantly, no bias or external forces were applied during the whole procedure so that both intermediates and products were completely free to sample configuration space in order to adapt to the plasticity of the active site and/or search for an exit. Differences in substrate reactivity were found to be correlated with the ease of adopting the near-attack conformation and two different exit pathways were found for product release that do not interfere with substrate entrance. Additional support for the different entry and exit pathways was independently obtained from an examination of the enzyme's normal modes.

Keywords: Dehalogenases; Molecular dynamics; Enzyme mechanism; Quantum mechanics; Molecular graphics; Normal mode analysis

1. Introduction

Synthetic halogenated alkanes and alkenes constitute an important class of soil and ground water pollutants because (i) they are continuously created in industrial processes as both products and byproducts, (ii) they are widely used in industry and agriculture, and (iii) they tend to persist in the environment due to their poor biodegradability. Nevertheless, microbial communities exposed to these substances often respond by expressing specific catabolic pathways that degrade these molecules in order to exploit them as growth substrates. The key enzymes in this catabolism are haloalkane dehalogenases (EC 3.8.1.5) which are compact globular proteins that belong to the structural superfamily of α/β hydrolases [1]. These enzymes remove halides from organic compounds, including polyhalogenated aliphatic hydrocarbons [2,3], via a hydrolytic mechanism that results in the production of the corresponding alcohol, inorganic halide, and hydrogen ion.

One such haloalkane dehalogenase, LinB, was originally isolated from a bacterial strain currently named *Sphingobium japonicum* (formerly, *Sphingomonas paucimobilis*) UT26 [4], and is the second enzyme in the biochemical pathway that enables this bacterium to utilize the useful but infamous insecticide γ-hexachlorocyclohexane (Lindane) as its sole carbon and energy source [5]. LinB also catalyses, in the absence of any cofactor except water, the conversion of a broad range of halogenated alkanes to their corresponding alcohols [4] which makes it of particular interest for bioremediation purposes. Substrate specificity has been shown to depend non-linearly on the size of the substrate molecules [6] and to be related to the fact that the active site in LinB is much larger than in other dehalogenases such as DhlA from *Xanthobacter autotrophicus* GJ10 or DhaA from *Rhodococcus* sp. [7]. Most noteworthy, 1,2-dichloroethane (DCE) is not only a very poor substrate (0.012 nmol s^{-1} mg of $enzyme^{-1}$) but also a simple competitive inhibitor of other substrates [8] whereas the

* Corresponding author. Tel.: +34 918854514; fax: +34 918854591.
E-mail address: federico.gago@uah.es (F. Gago).

1093-3263/$ – see front matter © 2007 Elsevier Inc. All rights reserved.
doi:10.1016/j.jmgm.2007.03.010

slightly larger 1,2-dibromoethane (DBE) is effectively debrominated to bromoethanol [6].

LinB has 296 amino acid residues that are organized into two structural domains, a larger one made up of an eight-stranded β-sheet flanked by α-helices and a smaller cap helical domain containing extensive loops [9,10]. The active site which is an occluded and mostly hydrophobic cavity located between the two domains, includes the catalytic triad (Asp108, His272 and Glu132) [11] and is connected to the surface and the bulk solvent by two possible export/import routes usually referred to as the ''main tunnel'' and the ''slot'', both of which have been studied in detail with the CAVER tool [12].

Three structural features of haloalkane dehalogenases have been recognized as essential for its catalytic performance: (i) the catalytic triad, (ii) an oxyanion hole, and (iii) the halide-stabilizing residues [13,14]. In the case of LinB, the carboxylate of Asp108 performs the nucleophilic attack on the alpha-carbon of the substrate which results in cleavage of the carbon–halogen bond by an S_N2 displacement mechanism that gives rise to the halide and an alkyl-ester intermediate. His272 and Glu132 are crucial residues in the subsequent step, when this intermediate is hydrolyzed by a water molecule. The carboxylate of Glu132 helps the imidazole ring of His272 to keep its proper orientation by establishing an OE1–Nδ hydrogen bond while at the same time it also increases the basicity of Nε (thus allowing this nitrogen to activate the hydrolytic water through the abstraction of a proton) and stabilizes the positive charge that develops on the imidazole ring of His272 during this second reaction. The side chains of two additional amino acids, Asn38 and Trp109, are involved in the stabilization of the leaving halide in the transition state (TS) of the first S_N2 reaction through hydrogen bonding interactions. This halide anion, together with a proton and the corresponding primary alcohol, are the products created during the reaction, and they have to exit the active site to make room for a new substrate molecule. Although much computational work has been devoted to understanding the energetics of the dehalogenation reaction (for a review, see reference [15]), comparatively little has been done in terms of trying to provide mechanistic insight about the motions of both reactants and products into and out of the active site.

The kinetic mechanism of LinB has been extensively studied using both steady-state and presteady-state kinetic techniques. The proposed reaction cycle (Scheme 1) is initiated by binding of the substrate in the Michaelis complex (E·RX), followed by the nucleophilic attack and formation of halide and the alkyl-enzyme intermediate (E-R·X^-) that is subsequently hydrolyzed to form the corresponding alcohol (E·ROH·X^-). This latter reaction has been shown to be the rate-limiting step in LinB acting on chlorocyclohexane, bromocyclohexane and 1-chlorohexane, and no dependence on the presence of one of the products for release of the other product has been detected which suggests a random sequential mechanism for exiting the enzyme [16].

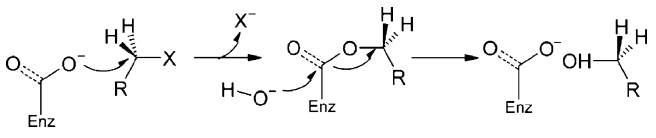

Scheme 1.

In an attempt to understand the full catalytic cycle of LinB in atomic detail and the reasons for the widely different catalytic rates on different substrates, we have examined the flexibility of the enzyme and simulated the reaction mechanism by using a combination of normal mode analysis (NMA), quantum mechanics (QM), molecular mechanics (MM), and molecular dynamics (MD) methods. As a model substrate we have chosen DBE although, for comparison purposes, we have also applied the same procedure to DCE, a very poor substrate, and 3-chloro-2-(chloromethyl)-1-propene (CCMP), one of the best substrates for LinB studied so far [6]. Thus, we were able to obtain a complete set of snapshots describing the sequence of events that lead from E·RX to E·ROH·X^- and product release.

2. Methodology

2.1. Quantum mechanical methods, molecular mechanics force field and point charges

The structures of the halogenated substrates and S_N2 reaction intermediates were built using the molecular modeling package Insight II [17]. Their geometries were first refined by means of the semiempirical QM program MOPAC [18], using the AM1 Hamiltonian and PRECISE stopping criteria, and further optimized using a restricted Hartree–Fock (RHF) method and a 6–31G(d) basis set, as implemented in the ab initio program Gaussian 03 [19]. The calculated wavefunctions were used to derive electrostatic potential-derived (ESP) charges employing the RESP methodology [20] for (i) the substrates in the ground state, (ii) the S_N2 transition states using acetate anion as a surrogate of Asp108, (iii) the Asp108-bound alkyl intermediates, and (iv) the corresponding haloalcohols. Equilibrium bond lengths and angles were obtained by averaging equivalent terms from the ab initio 6–31G(d) energy-minimized structures. Dihedral parameters for the Br_1–C_2–C_3–Br_4 torsion around the central C–C bond in DBE were calculated so as to reproduce, in the AMBER force field using SPASMS [21], the torsional barrier calculated ab initio in Gaussian 03 (keyword SCAN) upon rotation of the bond every 15°, as reported previously for DCE and similar molecules [22]. The nonbonded parameters used for Cl and Br atoms have already been shown to reproduce accurately the densities and enthalpies of vaporization of liquid DCE and bromoethane at 300 K [22]. The halides were given a charge of −1. The remaining bonded and nonbonded parameters were assigned, by analogy or through interpolation from those already present in the AMBER database, in a way consistent with the second-generation AMBER force field [23] (parm99). The van der Waals radii and nonbonded parameters for the halogens in the TS were the mean values between those for the atoms and those for the anions.

The S_N2 attack by Asp108 was simulated by progressively reducing (in 0.05 Å decrements) the distance separating the nucleophilic oxygen of a model acetate ion and the carbon at

position 2 of each substrate using the AM1 Hamiltonian as implemented in MOPAC [18]. The total charge of the system was set to −1 and atom positions were specified in internal coordinates. The geometry corresponding to a maximum in the heat of formation along this reaction path was used as input to locate and characterize the TS (keywords TS and FORCE) which was shown to possess only one negative eigenvalue. The calculated vibrations were visualized in MOLDEN [24]. The AM1-optimized TS structures were subsequently employed as initial guesses for the location of the TS geometries in Gaussian 03 using the synchronous transit-guided quasi-Newton (STQN) method and the RHF/6–31G(d) level of theory. Vibrational frequencies were then calculated to ensure that the calculated geometry for each TS had only one imaginary frequency that was associated with the dehalogenation reaction. These calculations also allowed us to characterize the ground state conformer that best resembled the TS in terms of both van der Waals contact distance between the two reacting atoms and angle of approach (i.e. the so called near-attack conformation, NAC) [25].

2.2. Model building, normal mode analysis and cavity calculations

The 1.8 Å X-ray crystal structure of the LinB–DCE complex (PDB code 1G5F) [8] was retrieved from the Protein Data Bank [26]. To probe the flexibility of this enzyme, an elastic network model was used in which all non-hydrogen protein atoms (within a cutoff of 10 Å) were modeled as point masses and Cα atoms were connected by springs representing the interatomic force fields [27]. LinB protein was then analyzed as a large set of coupled harmonic oscillators using the NOMAD-Ref server [28]. The conformational changes most likely involved in substrate entry and product release were deduced by calculating the 10 lowest-frequency normal modes which are those with the highest amplitudes and those most often related to large-scale structural rearrangements in proteins. Each mode was explored in its two opposite directions, thus resulting in two structures (''open'' and ''closed'') different from the crystallographic structure within an rmsd value of 2 Å.

The areas and volumes of pockets located on the protein surface as well as the voids buried in the protein interior were calculated analytically by means of the CASTp server [29] whereas the CAVER server [12] was employed to delineate the shape of the main tunnel and the slot connecting the active site with the bulk solvent.

For modeling the three Michaelis complexes studied in the present investigation, the poor DCE substrate (which is found in the crystal at the tunnel entrance in two possible orientations, each with a fractional occupancy of 50%) was replaced by either DBE or CCMP using the computer graphics program Insight II [17]. To avoid any bias, both DCE and DBE were modeled as low-energy *trans* conformers. Polar and non-polar hydrogen atoms in the protein were added using the program WHATIF 5.0 [30]. The carboxylic groups of Asp108 and Glu132 were deprotonated and His272 was singly protonated on Nδ, in accordance with the catalytic function of these residues.

2.3. Molecular dynamics simulations

The MD simulations were carried out using the AMBER 8.0 suite of programs [21]. Each molecular system was neutralized by the addition of sodium ions [31], and immersed in a rectangular box of ∼8550 TIP3P water molecules [32]. Periodic boundary conditions were applied and electrostatic interactions were treated using the smooth particle mesh Ewald method [33] with a grid spacing of 1 Å. The cutoff distance for the nonbonded interactions was 9 Å. The SHAKE algorithm [34] was applied to all bonds and an integration step of 2.0 fs was used throughout. Solvent molecules and counterions were relaxed by energy minimization and then allowed to redistribute around the positionally restrained solute (25 kcal mol^{-1} $Å^{-2}$) during a 50-ps run of MD at constant temperature (300 K) and pressure (1 atm). These initial harmonic restraints were gradually reduced in a series of progressive energy minimizations until they were completely removed. The resulting systems were heated again from 100 K to 300 K during 20 ps and allowed to equilibrate in the absence of any restraints for 10.0 ns during which system coordinates were collected every 2 ps for further analysis.

Upon achievement by the substrate of the NAC, the geometry of the atoms making up the TS was replaced by that of the quantum mechanically calculated TS of the S_N2 reaction, and the AMBER topology file was updated with the new bond and atom type definitions. A short energy minimization using this redefined topology allowed this geometry within the active site to be optimized in the MM force field. The MD simulation continued thereafter using the new topology but retaining the former atom velocities to sample the configuration space of the enzyme-TS complex during 10 ns. We found it necessary to turn off the SHAKE algorithm and use an integration time step of 1 fs for the first 20 ps to allow for bond readjustments. This trajectory, which proved to be very stable, provided a representative snapshot of the enzyme-TS complex, the topology of which was modified again by assigning the Cl^- or Br^- parameters to the leaving chloro or bromo atom (thus converting it into an anion) and defining a covalent bond between OD1 of Asp108 and C2 of the substrate. These new bonds were parameterized so as to reproduce the quantum mechanically optimized geometries, as explained above. Once again, atom velocities were kept, and equilibration of the E-R·X^- intermediate continued for another 10 ns under the same conditions as before. After that, water molecules in the vicinity of both His272 and Asp108 were monitored in search of the most suitable one for activation and hydrolytic attack on the ester bond. Next, a proton was transferred from this water molecule to His272 which became positively charged and was stabilized by the carboxylate of Glu132, whereas the hydroxyl anion was attached to CG of Asp108 to yield the transient negatively charged tetrahedral intermediate that is stabilized by the 'oxyanion hole'. This updated system was refined by carrying out an energy minimization until the root-mean-square deviation of the energy gradient was less than 0.1 kcal mol^{-1} $Å^{-1}$. Subsequent modeling of the products formed upon collapse of this oxyanionic intermediate yielded the final

complex which consisted of the halide, a neutral singly protonated His272, a deprotonated Asp108 and the free alcohol. This latter complex was energy-minimized as before, and then simulated for 10 ns of MD under the conditions described above to probe the exit routes that allow both products to be released into the bulk solvent. Note that a detailed quantum mechanical treatment of the resolution of the second TS of the reaction, i.e. collapse of the tetrahedral intermediate and proton transfer, is not reported here as this will be the focus of a separate piece of work.

2.4. Analysis of molecular dynamics trajectories

Three-dimensional structures and trajectories were visually inspected using the computer graphics program PyMOL [35]. Interatomic distances and angles, as well as root-mean-square deviations (rmsd) from a given structure, were monitored using the CARNAL module in AMBER.

3. Results and discussion

The five reaction steps that were investigated during the MD simulations using DBE as the substrate can be described as follows: (i) equilibration of the LinB·DBE Michaelis complex and adoption of the NAC for the S_N2 reaction, (ii) stabilization of the resulting TS within the active site, (iii) simulation of the complex containing the halide ion and the covalent alkyl-enzyme intermediate, (iv) activation of the water molecule that leads to hydrolysis of the ester, and (v) exit of the products from the active site (Fig. 1). The results will be presented and discussed for each of these steps in turn.

(i) *Equilibration of the LinB·DBE Michaelis complex and adoption of the NAC*. Despite the fact that in our initial model DBE was found in a *trans* conformation at the tunnel entrance (Fig. 1A), the initial energy minimization resulted in deeper penetration of the substrate into the active site and a change of the Br_1–C_2–C_3–Br_4 dihedral angle from *trans* to *gauche* (−), in agreement with previous automated docking calculations [6]. We relate this observation to the fact that the proximity of C_2 to Asp108(OD1) and orientation of the Br_1–C_2 bond dipole in the electrostatic field within the active site entails the electrostatic repulsion of Br_4, and this is minimized by the torsional change.

Further accommodation of DBE in the active site of LinB during the ensuing MD simulation did not require any major structural rearrangements as the side chains of Ile134, Phe143, Leu150, Phe151, Phe154, Phe169, Val173, Pro208, Ile211, and Leu248 provide a suitable hydrophobic environment for substrate binding and in-line positioning of the C_2–Br_1 bond with respect to the catalytic Asp, that is, adoption of the NAC [25] which allows the reaction to proceed. In common with reports for another dehalogenase, we consider that for NAC stabilization the following three conditions need to be simultaneously fulfilled: (i) a distance between the nucleophilic oxygen (OD1) of Asp108 and the attacked carbon of DBE (C2) $\leq$ 3.4 Å, (ii) an angle between OD1 of Asp108, C2 and the leaving halogen between 157° and 180° [36], and (iii) adequate stabilization of the leaving halogen by hydrogen bonding interactions with the side chain nitrogens of Asn38 and Trp109 which assist in formation of the halide by further polarizing the C_2–Br_1 covalent bond.

The NAC conformation was repeatedly adopted by DBE during the first ns of MD simulation (Fig. 1B) but it was lost thereafter, in agreement with the view that pre-TS steps are usually reversible, and substrates often diffuse in and out of the catalytic site many times before catalysis [37]. Each of these NACs can, in principle, progress toward the TS. Although the *gauche* (+) conformer was also observed, only the *gauche* (−) conformer of DBE was associated with a productive NAC because the former was not compatible with a suitable in-line orientation for attack by Asp108(OD1). This substrate is able to benefit from substantial conformational freedom within the active site because of three main factors: (i) the electrostatic repulsion between each bromine in DBE and the carboxylate of Asp108, (ii) competing electrostatic attraction between the bromine atoms and the amide nitrogen (ND2) of Asn38 and/or the indole nitrogen (NE1) of Trp109 on the one hand (Fig. 2) and the aromatic edges of Phe151 and Phe169 on the other hand, and (iii) the relatively large size of the active site in this dehalogenase (319.5 $Å^3$ in LinB versus 128.0 $Å^3$ in DhlA [38], as calculated by CASTp for the crystal structures of the apoenzymes: 1CV2 and 1EDE, respectively). Importantly, we note that whereas the indole ring of Trp109 is firmly anchored in position mostly due to a buttressing stacking interaction from Trp207, the carboxamide of Asn38 is relatively free to rotate, especially when no halide is bound and the size of the substrate is relatively small, as is the case for DBE. This rotation allows this group to establish good hydrogen bonds with either one of the substrate halogens or one of the water molecules that partially solvate the active site.

(ii) *TS stabilization within the active site*. Shortening of the Asp108-OD1...DBE–C_2 distance from 4.5 Å to 1.8 Å in the QM calculation on the model system resulted in two different TS structures, depending on whether the initial *gauche* conformation of the substrate was + or −. The Br_1–C_2–C_3–Br_4 torsion angle was ±86.4° when the AM1 Hamiltonian was used and ±91.9° when the calculation was performed with a 6–31(d) basis set. In the latter case, the vibrational analysis showed only one imaginary frequency (−485.765 cm^{-1}) in both *gauche* (+) and *gauche* (−) conformations of the TS that corresponded to the breaking/formation of the Br_1–C_2/C_2–OD1 bond.

When the *gauche* (−) TS structure was incorporated into the active site and the system was allowed to relax using MM, no major structural readjustments were detected on the part of the enzyme. Adaptation of LinB to accommodate the TS structure involved only minor rearrangements that resulted in improved contacts with the

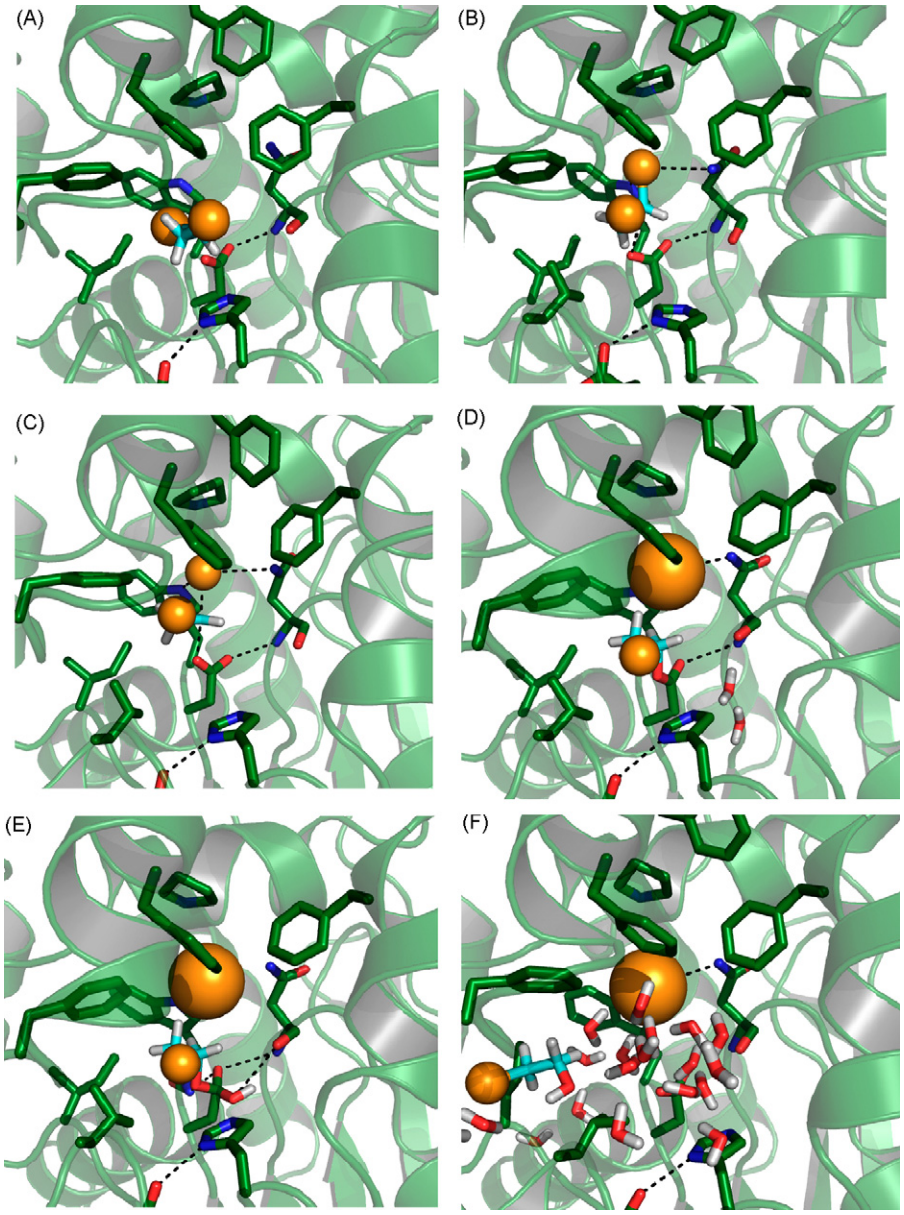

Fig. 1. Representative snapshots from the MD simulations displaying the conversion of DBE (cyan sticks and orange spheres for the halogen atoms) to bromoethanol and bromide ion (large orange sphere) that is catalyzed by LinB (green ribbon representation and atom type colored sticks for selected residues): (A) DBE at the tunnel entrance, (B) adoption of the NAC, (C) stabilization of the TS within the active site, (D) newly formed bromide ion and water molecules near the covalent alkyl-enzyme intermediate, (E) stabilization of the tetrahedral intermediate that results from the hydrolytic attack of the ester by a water molecule, and (F) filling of the active site with water molecules in the presence of both the bromide and the bromoethanol. See text for details.

side chains of a number of amino acids lining the active site. In the first place, the distances between the leaving halogen (Br_1) and Trp109(NE1) and Asn38(ND2) were shortened to 3.7 ± 0.2 Å and 3.6 ± 0.2 Å, respectively. In addition, Br_1 was found to be in very close van der Waals contact with the edges of the aromatic rings of Phe151 (HE2) and Phe169 (HZ), as well as with the pyrrolidine ring of Pro208 (HA and HB2), all of which provided additional stabilization. On the other hand, the other halogen atom (Br_4) appeared to fit snugly into a pocket made up by the side chains of Leu248 and Ile134 whereas the *s*-butyl of Ile211 was found in between the two halogen atoms, thus minimizing the repulsion between them. The Asp108(OD1)-DBE(C_2)-DBE(Br_1) in-line orientation remained very stable during the MD simulation of this complex, with an average angle of approach of $176.5 \pm 1.7^\circ$, strongly suggesting that the atom arrangement obtained faithfully represents the conformation of the enzyme-TS complex (Fig. 1C).

(iii) *Complex containing the halide ion and the covalent alkyl-enzyme intermediate*. The in situ formed bromide ion was extremely stable in its binding pocket (Fig. 1D) and maintained its interaction with Trp109(NE1) and Asn38(ND2) (3.6–3.7 Å) during the 10 ns of MD simulation, most likely because of the enhanced electrostatic attraction brought about as a consequence of the

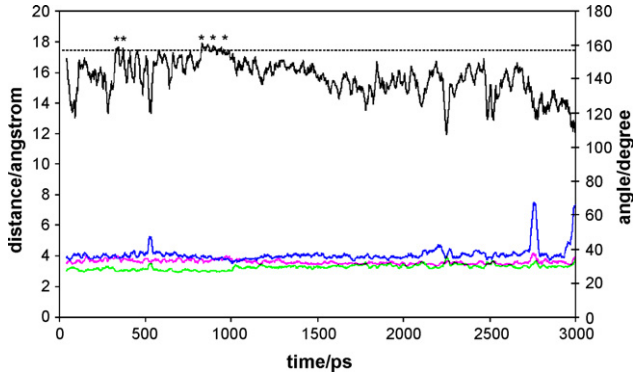

Fig. 2. Assessment of near-attack conformation (NAC, asterisks) accomplishment by DBE in the active site of LinB over the simulation time. NAC formation was monitored by measuring Asn38(ND2)···DBE(Br_1) (magenta), Asp108(OD1)···DBE(C_2) (green), Trp109(NE1)···DBE(Br_1) (blue) distances and the Asp108(OD1)···DBE(C_2)···DBE(Br_1) angle (black). The 157° threshold for this angle is indicated by the dotted line.

negative charge on the ion. Once again, no major enzyme structural rearrangements were observed when the complex containing the halide and the haloalkylated Asp108 in the active site were simulated except for minor geometry readjustments. Most notably, transferring the negative charge from the catalytic aspartate to the leaving anion, with the ensuing expansion of the atomic radius of bromine to the ionic radius of bromide, did not bring about any significant readaptation of amino acid side chains within the active site although it obviously had an influence on the electrostatics, as mentioned before, and in the recalculation of the forces thereafter. This observation is in consonance with crystallographic findings showing that the active site cavity, which is virtually identical in the LinB apoenzyme [9] and in the complexes with different substrates [8,39], always contains a halide ion at close distance of both Trp109 and Asn38 when the dehalogenation reaction has taken place.

The OD1–C_2–C_3–Br_4 torsion angle in the alkyl intermediate was seen to vary during the subsequent MD equilibration. In our view, this finding reflects the fact, once again, that the large volume available for this small substrate in the active site of LinB does not completely freeze the reactant atoms. As a consequence, this mobility is likely to slow down further progression of the S_N2 reaction toward the final products and can explain why small linear haloalkanes are usually worse substrates for LinB than longer (e.g. 1-chlorohexane) or cyclic ones (e.g. chlorocyclohexane) [6,16].

Since a water molecule is necessary for breaking down this covalent intermediate, water molecules within and around the active site were monitored. One particular water molecule was present during the whole length of the simulation in a position equivalent to that of the highly conserved crystallographic water molecule observed in all the LinB structures reported to date (WAT48 in 1G5F). This water bridges the gap between the carbonyl oxygen of Asn38 and Nε of His272 and is held in position by a second water molecule that is, in turn, hydrogen bonded to Nδ of His107, Oγ of Thr40, and the NH of Gly37 (WAT9 in 1G5F). In this orientation, the oxygen atom is ready for the nucleophilic attack on Asp108 CG upon activation by His272. Interestingly, these two water molecules not only display relatively low B-factors in the crystal (<10 $Å^2$) but also show long residence times during the MD simulation (data not shown) which is consistent with their important role in catalysis.

(iv) *Activation of the water molecule and hydrolysis of the ester.* The snapshot selected from the previous step provided the input coordinates for the next geometry. The water proton hydrogen bonded to His272 was transferred to the Nε of this amino acid which thus became positively charged, whereas the hydroxyl anion served to generate the transient tetrahedral intermediate, as explained above. This oxyanion was stabilized through hydrogen bonding to the backbone amide nitrogens of Trp109 and Asn38 (Fig. 1E).

(v) *Exit of the products from the active site*. Up to this point, the bromide anion had remained in the location where it was generated due to the very close interactions that it established with the nitrogens of Trp109 and Asn38, as well as the pyrrolidine ring of Pro208 and the edges of the aromatic rings of Phe151 and Phe169. On the other hand, the bromoethanol hydroxyl group was initially hydrogen bonded to the OD1 carboxylate of Asp108. However, as a result of the progressive solvation of the active site during the MD simulation of the E·ROH·X^- complex, the number of water molecules making up the first hydration shell of both the anion and the alcohol started to increase (Fig. 1F). As a result, the interaction between the bromide and the halide-stabilizing residues weakened along the trajectory as did that between the alcohol and the aspartate. Eventually, both products started to leave the active site cavity (Fig. 3), first (at about 5 ns) the alcohol through the slot (lined by residues Ile138, Asp142, Pro144, Ala247, Leu248, Thr250, Gly251, and Arg252) and then (at about 7.5 ns) the fully solvated bromide through the upper part of

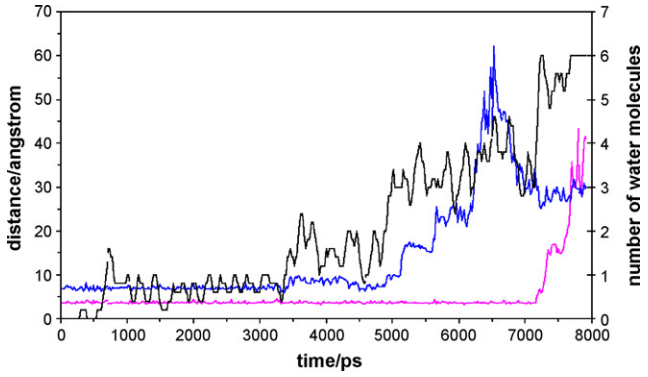

Fig. 3. Evolution of the distances (Å) between Trp109(NE1) and either the bromide ion (magenta) or the hydroxyl group of bromoethanol (blue) during the first 8 ns of MD simulation of product release. The number of water molecules surrounding the bromide ion as it moves from the active site towards the bulk solvent is shown by the black line which represents average values calculated over 100-ps windows.

the main tunnel (lined by residues Gln146 and Asp147). Remarkably, the highest amplitude of essential motions of LinB has been reported to occur in the interdomain random coil that precedes helix α4 (residues Ala141–Arg148) [40].

We also noticed that the slot provides an exit pathway for some of the water molecules that gained access into the active site from the bulk solvent through the main tunnel. In fact, the bromoethanol product that leaves the site through this route is accompanied along the way by several water molecules, and in doing so it forces the side chain of Leu248 to rotate, a finding that is in good agreement with the disorder detected for the side chain of this amino acid in a high-resolution crystal structure of LinB [41].

The fact that product release could be observed during the 10 ns simulation through pathways that do not interfere with substrate entrance is in accord with the experimental verification that the exit of both halide and alcohol is a fast process and not a rate-limiting step as in the case of DhlA.[16]

3.1. Normal mode analysis and exit pathways

The low frequency motions of LinB were independently characterized by carrying out a normal mode analysis on the X-ray crystal structure. Examination of the normal modes for this enzyme revealed interesting fluctuations that were mostly located on the cap domain. Each mode was explored in its two opposite directions thus resulting in four structures (“open” and “closed” main tunnel, and “open” and “closed” slot) different from the initial one within an RMSD value of 2 Å. We thought that these conformational changes could be of relevance for our studies because they define two important entrance/exit pathway into/from the enzyme. In fact, exploration with the CAVER algorithm [12] of the structures obtained from the NOMAD-Ref server [28] revealed that the simulated motions in LinB clearly expand the hydrophobic tunnels connecting the active site cavity with the bulk solvent, especially when the second normal mode is considered (Fig. 4). These are the same tunnels that were identified during the MD simulations reported above as entrance/exit pathways for substrates, products and water molecules. Taken together, these findings suggest that this specific mode is directly coupled to the biochemical reaction.

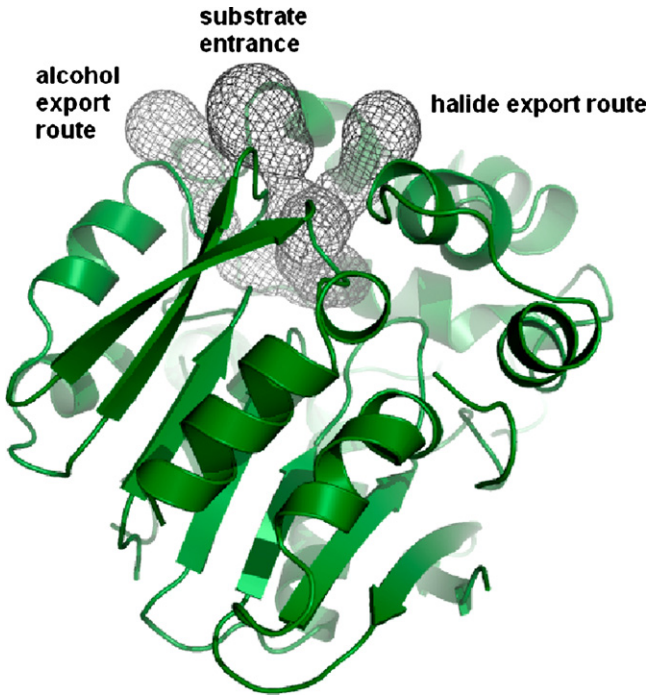

Fig. 4. Schematic representation of LinB (green ribbon) showing the different import/export pathways (grey mesh) characterized with CAVER [12] using the atomic coordinates of LinB generated by NOMAD-Ref [28] for the second normal mode.

3.2. Comparative MD studies with other substrates

The same MD protocol was applied to the complexes of LinB with DCE and CCMP which behave as much worse and better substrates, respectively, than DBE in terms of both K_M and k_{cat} [6]. In the case of DCE, and contrary to what was observed for the highly similar DBE, the NAC conformation was not achieved during the 10 ns of simulation. This was so because not all the conditions were simultaneously fulfilled, not even during the first 3 ns prior to return to the main entrance tunnel (Fig. 5) and despite the observation that one of the two chloro atoms was always close to the Asn38 nitrogen. In fact, one factor that can account for these findings, and also for the fact that the k_{cat} for DCE is at least four orders of magnitude smaller than for DBE (manuscript in preparation), is the greater competition between these two halogen atoms to interact with the carboxamide nitrogen of Asn38, as well as the greater repulsion from Asp108(OD1) that results from the more negative partial charges on the chloro atoms relative to the bromo atoms. Furthermore, the halide-stabilizing residues appear to be better solvated when the substrate is DCE than when it is DBE. Consequently the tumbling of this substrate inside the active site in a variety of non-productive orientations has the additional effect of blocking the entrance of other substrates by a competitive mechanism which is

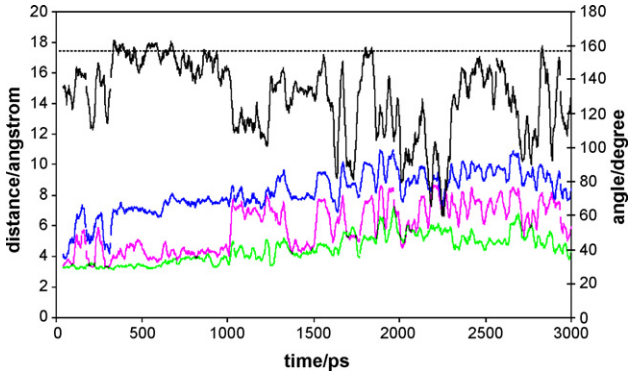

Fig. 5. Lack of adoption of near-attack conformation by DCE in the active site of LinB over the simulation time, as monitored by measuring Asn38(ND2)···DCE(Cl_1) (magenta), Asp108(OD1)···DCE(C_2) (green), Trp109(NE1)···DCE(Cl_1) (blue) distances and the Asp108(OD1)···DCE(C_2)···DCE(Cl_1) angle (black). The 157° threshold for this angle is indicated by the dotted line.

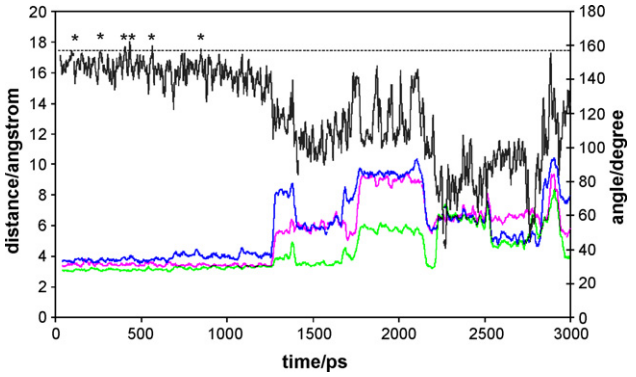

Fig. 6. Assessment of near-attack conformation (NAC, asterisks) accomplishment by CCMP in the active site of LinB over the simulation time. NAC formation was monitored by measuring Asn38(ND2)···CCMP(Cl_1) (magenta), Asp108(OD1)···CCMP(C_2) (green), Trp109(NE1)···CCMP(Cl_1) (blue) distances and the Asp108(OD1)···CCMP(C_2)···CCMP(Cl_1) angle (black). The 157° threshold for this angle is indicated by the dotted line.

in agreement with the experimental data showing that DCE acts as a simple competitive inhibitor of other substrates such as 1-chlorobutane [8].

As regards CCMP, the NAC was achieved several times during the simulation of this substrate within the active site of LinB (Fig. 6) and, again, this relatively small molecule was able to move back into the entrance tunnel. This happened after only 1 ns in this case and was related to the rapid entry of a water molecule that competed with CCMP for hydrogen bonding to Trp109(NE1) and Asn38(ND2).

In view of all of the above results, a correlation does appear to exist between the number of NACs that the substrate molecule can form in the Michaelis complex (each of which can instantaneously progress to a TS) and the catalytic rate enhancement that is observed experimentally, as suggested for other enzymes [42].

4. Conclusions

In the present work, we have characterized the different steps of the dehalogenation reaction carried out by LinB on three different substrates using standard MD simulations. This has allowed us to obtain information in atomic detail about each step of the catalytic mechanism, that is, substrate entrance into the active site pocket, achievement of the NAC, stabilization of the S_N2 reaction TS followed by halide release, water molecule activation and subsequent hydrolytic attack on the ester intermediate with delivery of the alcohol, and finally product release. Importantly, no bias or external forces were applied during the whole procedure so that both intermediates and products were completely free to sample configuration space in order to adapt to the plasticity of the active site and/or search for an exit.

We found that the highly preorganized catalytic site of LinB provides an anisotropic and dynamic electronic environment that increases the probability that the TS of the dehalogenation reaction will be formed. Nonetheless, due to relatively weak binding forces in the active site and possible competing interactions with water molecules, it was apparent that the substrates need to spend some time trying to adjust their conformations in order to achieve the close van der Waals contacts and the proper alignment of the reactants' orbitals that are necessary for the reaction to proceed. This process varied from one substrate to another and the active site architecture ensured that a suitable conformer subpopulation (e.g. *gauche*—in the case of DBE substrate ensemble) was selected to achieve the NAC.

It was shown that the motions required for the formation and breakdown of the TS of the S_N2 reaction are minimal on the part of the enzyme, and also that the two products are released into the bulk solvent following two distinct exit pathways that are different from the substrate import route. Additional evidence for the existence of these three entry/exit pathways connecting the active site to the protein exterior was independently obtained from an examination of the enzyme's normal modes.

Acknowledgements

A North Atlantic Treaty Organization Linkage grant (EST.CLG.980504) is gratefully acknowledged, as well as financial support to J.D. from the Czech Ministry of Education (MSM0021622413) and to F.G. from the Spanish Ministry of Education and Science (SAF2003-07219-C02-02 and SAF2006-12713-C02-02).

References

[1] M. Holmquist, Alpha/beta-hydrolase fold enzymes: structures, functions and mechanisms, Curr. Protein Pept. Sci. 1 (2000) 209–235.
[2] S. Fetzner, F. Lingens, Bacterial dehalogenases: biochemistry, genetics, and biotechnological applications, Microbiol. Rev. 58 (1994) 641–685.
[3] S. Fetzner, Bacterial dehalogenation, Appl. Microbiol. Biotechnol. 50 (1998) 633–657.
[4] Y. Nagata, K. Miyauchi, J. Damborsky, K. Manova, A. Ansorgova, M. Takagi, Purification and characterization of a haloalkane dehalogenase of a new substrate class from a gamma-hexachlorocyclohexane-degrading bacterium, *Sphingomonas paucimobilis* UT26, Appl. Environ. Microbiol. 63 (1997) 3707–3710.
[5] Y. Nagata, T. Nariya, R. Ohtomo, M. Fukuda, K. Yano, M. Takagi, Cloning and sequencing of a dehalogenase gene encoding an enzyme with hydrolase activity involved in the degradation of gamma-hexachlorocyclohexane in *Pseudomonas paucimobilis*, J. Bacteriol. 175 (1993) 6403–6410.
[6] J. Kmunicek, K. Hynkova, T. Jedlicka, Y. Nagata, A. Negri, F. Gago, R.C. Wade, J. Damborsky, Quantitative analysis of substrate specificity of haloalkane dehalogenase LinB from *Sphingomonas paucimobilis* UT26, Biochemistry 44 (2005) 3390–3401.
[7] T. Bosma, M.G. Pikkemaat, J. Kingma, J. Dijk, D.B. Janssen, Steady-state and pre-steady-state kinetic analysis of halopropane conversion by a *Rhodococcus* haloalkane dehalogenase, Biochemistry 42 (2003) 8047–8053.
[8] A.J. Oakley, Z. Prokop, M. Bohac, J. Kmunicek, T. Jedlicka, M. Monincova, I. Kuta-Smatanova, Y. Nagata, J. Damborsky, M.C. Wilce, Exploring the structure and activity of haloalkane dehalogenase from *Sphingomonas paucimobilis* UT26: evidence for product and water-mediated inhibition, Biochemistry 41 (2002) 4847–4855.
[9] J. Marek, J. Vevodova, I. Smatanova, Y. Nagata, L.A. Svensson, J. Newman, M. Takagi, J. Damborsky, Crystal structure of the haloalkane dehalogenase from *Sphingomonas paucimobilis* UT26, Biochemistry 39 (2000) 14082–14086.
[10] D.L. Ollis, E. Cheah, M. Cygler, B. Dijkstra, F. Frolow, S.M. Franken, M. Harel, S.J. Remington, I. Silman, J. Schrag, The alpha/beta hydrolase fold, Protein Eng. 5 (1992) 197–211.

[11] K. Hynkova, Y. Nagata, M. Takagi, J. Damborsky, Identification of the catalytic triad in the haloalkane dehalogenase from *Sphingomonas paucimobilis* UT26, FEBS Lett. 446 (1999) 177–181.
[12] M. Petrek, M. Otyepka, P. Banas, P. Kosinova, J. Koca, J. Damborsky, CAVER: a new tool to explore routes from protein clefts, pockets and cavities., BMC Bioinformatics 7 (2006) 316. http://loschmidt.chemi.muni.cz/caver.
[13] K.H. Verschueren, F. Seljee, H.J. Rozeboom, K.H. Kalk, B.W. Dijkstra, Crystallographic analysis of the catalytic mechanism of haloalkane dehalogenase, Nature 363 (1993) 674–675.
[14] J. Damborsky, J. Koca, Analysis of the reaction mechanism and substrate specificity of haloalkane dehalogenases by sequential and structural comparisons, Protein Eng. 12 (1999) 989–998.
[15] D.B. Janssen, Evolving haloalkane dehalogenases, Curr. Opin. Chem. Biol. 8 (2004) 150–159.
[16] Z. Prokop, M. Monincova, R. Chaloupkova, M. Klvana, Y. Nagata, D.B. Janssen, J. Damborsky, Catalytic mechanism of the haloalkane dehalogenase LinB from *Sphingomonas paucimobilis* UT26, J. Biol. Chem. 46 (2003) 45094–45100.
[17] Insight II, version 98.0, Molecular Simulations Inc., San Diego, CA, USA 1998.
[18] J.J.P. Stewart, MOPAC: a semiempirical molecular-orbital program, J. Comput. Aided Mol. Des. 4 (1990) 1–45.
[19] M.J. Frisch, G.W. Trucks, H.B. Schlegel, G.E. Scuseria, M.A. Robb, J.R. Cheeseman, V.G. Zakrzewski, J.A. Montgomery, R.E. Stratmann, J.C. Burant, Gaussian 03, revision B. 04, Gaussian Inc., Pittsburgh, PA, 2003.
[20] C.I. Bayly, P. Cieplak, W.D. Cornell, P.A. Kollman, A well-behaved electrostatic potential based method using charge-restraints for deriving charges: The RESP model, J. Phys. Chem. 97 (1993) 10269–10280.
[21] D.A. Case, T.E. Cheatham III, T. Darden, H. Gohlke, R. Luo, K.M. Merz Jr., A. Onufriev, C. Simmerling, B. Wang, R. Woods, The Amber biomolecular simulation programs, J. Comput. Chem. 26 (2005) 1668–1688.
[22] J. Kmunicek, S. Luengo, F. Gago, A.R. Ortiz, R.C. Wade, J. Damborsky, Comparative binding energy analysis of the substrate specificity of haloalkane dehalogenase from *Xanthobacter autotrophicus* GJ10, Biochemistry 40 (2001) 8905–8917.
[23] W.D. Cornell, P. Cieplak, C.I. Bayly, I.R. Gould, K.M. Merz, D.M. Ferguson, D.C. Spellmeyer, T. Fox, J.W. Caldwell, P.A. Kollman, A second-generation force field for the simulation of proteins, nucleic acids, and organic molecules, J. Am. Chem. Soc. 117 (1995) 5179–5197.
[24] G. Schaftenaar, J.H. Noordik, Molden: a pre- and post-processing program for molecular and electronic structures, J. Comput. Aided Mol. Des. 14 (2000) 123–134.
[25] S. Hur, T.C. Bruice, The near-attack conformation: approach to the study of the chorismate to prephenate reaction, Proc. Natl. Acad. Sci. U.S.A. 100 (2003) 12015–12020.
[26] H.M. Berman, J. Westbrook, Z. Feng, G. Gilliland, T.N. Bhat, H. Weissig, I.N. Shindyalov, P.E. Bourne, The Protein Data Bank, Nucl. Acids Res. 28 (2000) 235.
[27] E. Lindahl, M. Delarue, Refinement of docked protein–ligand and protein–DNA structures using low frequency normal mode amplitude optimization, Nucl. Acids Res. 33 (2005) 4496–4506.
[28] E. Lindahl, C. Azuara, P. Koehl, M. Delarue, NOMAD-Ref: visualization, deformation and refinement of macromolecular structures based on all-atom normal mode analysis, Nucl. Acids Res. (34 Web server issue) (2006) W52–W56. http://lorentz.immstr.pasteur.fr/nomad-ref.php.
[29] J. Dundas, Z. Ouyang, J. Tseng, A. Binkowski, Y. Turpaz, J. Liang, CASTp: computed atlas of surface topography of proteins with structural and topographical mapping of functionally annotated residues, Nucl. Acids Res. (34 Web server issue) (2006) W116–W118. http://cast.engr.uic.edu.
[30] G. Vriend, WHAT IF: a molecular modeling and drug design program, J. Mol. Graph. 8 (1990) 52.
[31] J. Aqvist, Ion water interaction potential-derived from free energy perturbation simulations, J. Phys. Chem. 94 (1990) 8021–8024.
[32] W.L. Jorgensen, J. Chandrasekhar, J.D. Madura, Comparison of simple potential functions for simulating liquid water, J. Chem. Phys. 79 (1983) 926–935.
[33] T.A. Darden, D. York, L.G. Pedersen, Particle mesh Ewald: an $N\cdot\log(N)$ method for Ewald sums in large systems, J. Chem. Phys. 98 (1993) 10089–10092.
[34] J.P. Ryckaert, G. Ciccoti, H.J.C. Berendsen, Numerical integration of the cartesian equations of motion of a system with constraints: molecular dynamics of *n*-alkanes, J. Comput. Phys. 23 (1977) 327–341.
[35] W. De Lano, DeLano Scientific LLC. PyMOL version 0.99. URL: http://www.pymol.org/.
[36] S. Hur, K. Kahn, T.C. Bruice, Comparison of formation of reactive conformers for the S_N2 displacements by $CH_3CO_2^-$ in water and by Asp124-CO_2^- in a haloalkane dehalogenase, Proc. Natl. Acad. Sci. U.S.A. 100 (2003) 2215–2219.
[37] V.L. Schramm, Enzymatic transition states and transition state analogues, Curr. Opin. Struct. Biol. 15 (2005) 604–613.
[38] M.G. Pikkemaat, I.S. Ridder, H.J. Rozeboom, K.H. Kalk, B.W. Dijkstra, D.B. Janssen, Crystallographic and kinetic evidence of a collision complex formed during halide import in haloalkane dehalogenase, Biochemistry 38 (1999) 12052–12061.
[39] V.A. Streltsov, Z. Prokop, J. Damborsky, Y. Nagata, A. Oakley, M.C. Wilce, Haloalkane dehalogenase LinB from *Sphingomonas paucimobilis* UT26: X-ray crystallographic studies of dehalogenation of brominated substrates, Biochemistry 42 (2003) 10104–10112.
[40] M. Otyepka, J. Damborsky, Functionally relevant motions of haloalkane dehalogenases occur in the specificity-modulating cap domains, Protein Sci. 11 (2002) 1206–1217.
[41] A. Oakley, M. Klvana, M. Otyepka, Y. Nagata, M.C.J. Wilce, J. Damborsky, Crystal structure of haloalkane dehalogenase LinB from *Sphingomonas paucimobilis* UT26 at 0.95 Å resolution: dynamics of catalytic residues, Biochemistry 43 (2004) 870–878.
[42] T.C. Bruice, A view at the millennium: the efficiency of enzymatic catalysis, Acc. Chem. Res. 35 (2002) 139–148.